NPL Report CMMT(A)198

Project PAJ2
Report No 12

Comparison of the Measured and Predicted Performance of Adhesive Joints under Impact

G Dean, G Lord and B Duncan

October 1999

ISSN 1361-4061

National Physical Laboratory
Teddington, Middlesex, UK, TW11 0LW

Approved on behalf of Managing Director, NPL, by Dr C Lea,
Head, Centre for Materials Measurement and Technology

CONTENTS

October 1999

Comparison of the Measured and Predicted Performance of Adhesive Joints under Impact

G Dean[x], G Lord[+] and B Duncan[x]

[x]Centre for Materials Measurement and Technology and
[+]Centre for Information Systems Engineering
National Physical Laboratory,
Teddington, Middlesex TW11 0LW

SUMMARY

The work reported here is concerned with predicting the performance of an adhesive joint under impact loading. Analyses of stress and strain distributions in a joint specimen were made using finite element methods for a range of speeds at which the specimen was loaded. Predictions of force against extension of the joint are compared with experimental data obtained up to failure of the specimen. The adhesive used was a toughened epoxy which was able to sustain large strains before failure. Elastic-plastic models have therefore been used in the FE analysis with materials parameters obtained from a variety of tests carried out in an earlier phase of the project. A wide range of deformation speeds has been employed in these tests to determine the strain rate dependence of mechanical properties.

Predictions of force against extension were made on a lap joint specimen whose dimensions were chosen with the intention of minimising plastic deformation of the adherends during a test. Solutions were obtained over a range of loading speeds using static and dynamic analyses with both standard and explicit solver codes. Predictions were compared with experimental data obtained under controlled deformation at slow speeds and under falling weight impact at higher speeds. Under impact loading, attempts have been made to interpret and model the transient forces that dominate the force/extension record at high speeds.

Calculations have also been made of strain components in the region of strain concentration in the adhesive where specimen failure is expected to initiate. Strain levels are compared with a failure criterion developed in a earlier part of the project, and attempts are made to interpret the force/extension measurements in terms of partial failure of the adhesive prior to complete rupture of the joint.

1 INTRODUCTION

The objective of the work reported here is to explore the accuracy with which finite element methods can be used to predict the performance of an adhesive joint under impact loading. Finite element calculations have been made of force vs extension curves for a joint test specimen under different loading speeds and the strain distribution in the adhesive at failure. The latter is used to explore the validity of a failure criterion for adhesives developed from an analysis of tests on bulk and joint test-specimens (1).

The finite element calculations were made using elastic-plastic materials models. Identification of a suitable yield criterion for the adhesives being studied has been investigated in previous work (2) based on the results of tensile and shear tests on bulk specimens and tensile tests on butt-joint specimens. The tensile and shear tests on bulk specimens revealed that the von Mises yield criterion was not suitable for toughened adhesives, but they indicated that the linear Drucker Prager model seemed applicable. This model is based on a simple modification of the von Mises criterion to include some sensitivity of yielding to the hydrostatic component of stress. However, tensile tests on butt-joint specimens of an epoxy adhesive showed that the linear Drucker-Prager model was only approximately satisfactory over a limited range of stress states, implying that significant uncertainties may exist in the accuracy of stress and strain magnitudes calculated in regions of high dilatational stress that generally occur at stress concentrations where failure of the adhesive will initiate.

The exponent Drucker-Prager materials model was shown to be more realistic for the epoxy adhesive and was able to accurately predict the deformation behaviour of the butt-joint specimen using materials parameters derived from the tensile and shear tests on bulk specimens. However, this model was not suitable for correlating bulk and butt-joint specimen tests on an acrylic adhesive. Furthermore, estimations of volume changes derived from lateral strain measurements in tensile tests on bulk specimens led to the conclusion that a realistic model for toughened adhesives needs to take account of the contribution of rubber-particle cavitation, and maybe crazing of the polymer matrix, to the process of plastic deformation in the adhesive. The development of a more realistic model is the subject of further work.

In this report, the application of available elastic-plastic models to predicting the deformation behaviour of a test specimen having a single-lap-joint geometry is explored. The parameters for these models have been obtained in earlier work (2) from the bulk and butt-joint specimen tests just mentioned. For this purpose, constant strain rate tests have been performed over a range of strain rates to enable predictions to be made of joint performance under different speeds of deformation including impact. Finite element calculations have been made using standard (implicit) and explicit solver codes for both the quasi-static case (rate-independent data) and the dynamic case (rate-dependent data). Comparisons of force/extension curves are made with experimental results obtained with an epoxy adhesive. The magnitude and state of strain in the region of maximum strain in the adhesive are also calculated, and tentative comparisons are made with a failure criterion based on the results of other work (1).

2 THE JOINT TEST SPECIMEN

A lap shear test specimen geometry was chosen for the comparison of measured and predicted joint behaviour. A diagram showing the geometry and dimensions of the specimen is shown in figure 1. To improve the accuracy of strain predictions in the region of maximum strain in the adhesive, geometric singularities have been removed by incorporating a radius on the edge at the end of each adherend and a circular fillet on each end of the adhesive. The adherends were a steel grade chosen in conjunction with the thickness so that strain levels in the adherend during tests will be confined predominantly to the region for elastic behaviour.

The adhesive used in this study is a 1-part toughened epoxy supplied by Ciba Polymers with the code name LMD 1142.

3 DETERMINATION OF MATERIALS PARAMETERS

The properties of the epoxy adhesive required for finite element analyses using elastic-plastic models have been measured in an earlier phase of the project. These were obtained using a range of tests on bulk and joint test specimens, and the measurement methods and data analysis are described in reference (2). A summary of the data analysis for the determination of model parameters is given in this section.

3.1 ELASTIC PROPERTIES (E, ν_e)

The Young's modulus and Poisson's ratio were determined from measurements of stress, strain and lateral strain in tensile tests on bulk specimens at small strains where the stress-strain plot is linear. Values were observed to depend slightly upon the strain rate chosen for the test. Since there is currently no facility in Abaqus to include rate-dependent elasticity in elastic-plastic models, data for a single strain rate of 2.10^{-3} s^{-1} were used for the FE analyses. These data are shown in table 1.

Table 1. Properties of the epoxy adhesive at 23 ^oC used for finite element calculations

E (Gpa)	ν_e	λ	β	a (MPa^{-1})	ν_p	ψ	σ_T (ε_p) (MPa)
1.68	0.44	1.55	33^o	0.017	0.3	25^o	fig 2

3.2 STRAIN-HARDENING FUNCTION ($\sigma_T(\varepsilon_P)$)

The strain-hardening function was obtained from measurements of yield stress σ_T and plastic strain ε_p in a uniaxial tension test at strains ranging from that associated with the onset of non-linearity ($\varepsilon \approx 0.01$) up to the failure strain (typically $\varepsilon \geq 0.2$). Owing to the high strains involved, true stresses

and true strains were determined over the entire strain range. For strains above the linear range, the stress σ is identified with the yield stress σ_T and the true plastic strain component was calculated from the measured true strain assuming additivity of the elastic and plastic components (2).

The hardening function was determined over a range of strain rates, and data for the epoxy are plotted in figure 2.

3.3 HYDROSTATIC-STRESS SENSITIVITY PARAMETERS λ, β, a

The sensitivity of yielding to hydrostatic stress is characterised by the measured parameter λ which is the ratio of the yield stress in uniaxial compression σ_C to the yield stress in uniaxial tension determined at the same effective plastic strain and strain rate. The determination of the parameter λ requires measurements of the yield behaviour under two different stress states. If stress-strain data are available under both compression and tension, then λ may be obtained directly. However, owing to difficulties associated with uniaxial compression tests, values for λ have been determined in this project from a combination of tension and shear tests. This relies on the determination of yield stresses in shear σ_S and tension σ_T having the same effective plastic strain $\bar{\varepsilon}_p$ from stress/strain curves measured in shear and tension at the same effective plastic strain rate.

The parameter λ is then determined from the equation

$$\lambda = \frac{\sqrt{3}(\sigma_S / \sigma_T)}{2 - \sqrt{3}(\sigma_S / \sigma_T)} \qquad (1)$$

Equation (1) was used with pairs of yield stresses σ_S and σ_T over a range of values for the effective plastic strain to observe the variation of λ with strain. A representative value was selected at a strain rate of 2.10^{-3} s^{-1} and is recorded in table 1. A value for the parameter β, used in the expression in Abaqus for the linear Drucker-Prager yield criterion, was then derived using the equation

$$\tan\beta = \frac{3(\lambda - 1)}{\lambda + 1} \qquad (2)$$

In the exponent Drucker-Prager model, the parameter b in the Abaqus expression for the yield criterion was taken to have a value of 2. The parameter a was calculated using (see reference (2))

$$a = \frac{\sigma_T}{3(3\sigma_S^2 - \sigma_T^2)} = \frac{1}{3(\lambda - 1)\sigma_T} \qquad (3)$$

Once again, the parameter a for the epoxy is observed to depend experimentally upon plastic strain, and a representative value was selected as given in table 1. The parameter p_t, which characterises strain hardening behaviour, is given by

$$p_t = a\sigma_T^2 + \frac{\sigma_T}{3} \qquad (4)$$

where σ_T is a function of plastic strain and has been measured over a range of strain rates as shown in figure 2.

3.4 THE FLOW PARAMETER ψ

The flow parameter was determined from a representative value for the plastic component of Poissons ratio ν_p using the equation

$$\tan\Psi = \frac{3(1 - 2\nu_p)}{2(1 + \nu_p)} \qquad (5)$$

The values used for ν_p and ψ are given in table 1.

4 FINITE ELEMENT ANALYSES OF THE JOINT SPECIMEN

The mesh used in the analyses of the joint specimen is shown in figure 3. The mesh size was chosen such that the contour of maximum strain at an extension of 0.1 mm was greater than the size of the elements in the region of maximum strain. Preliminary results were obtained with a coarser mesh. The analyses assumed plane strain conditions in the specimen, and solutions have been obtained for a range of conditions in order to gain some level of confidence in the results.

4.1 A QUASI-STATIC ANALYSIS

The initial analyses were carried out under quasi-static conditions for which it is assumed that the properties of the adhesive are independent of the rate of loading and that this rate is sufficiently low that inertial forces are negligible. Solutions were obtained using the von Mises, the linear Drucker-Prager and the exponent Drucker-Prager models to describe the adhesive. The behaviour of the steel adherends was assumed to be linear elastic except in one of the analyses where solutions are presented allowing some plastic deformation of the steel. For these quasi-static analyses, hardening data from figure 2 were taken at a single strain rate of 115 s^{-1}. The specimen was loaded in the analyses by a stepwise increase of the extension at one end of the specimen (displacement control) whilst keeping the other end fixed. Results of force against extension obtained using each model are shown in figure 4. The extension is determined as the increase in the separation of points on the adherends either side of the joint having an initial separation of 25 mm. These correspond to points at which an extensometer is attached in experimental tests on the joint specimen (section 5).

It is apparent from figure 4 that the von Mises analysis gives lower predicted force values than the other models. This arises because the stress state in the adhesive is predominantly shear whilst the hardening function is determined from tensile data. Under these circumstances, a hydrostatic stress sensitive yield criterion is needed to obtain accurate predictions of behaviour in shear. Although the Drucker-Prager models have different dependencies of yielding on the hydrostatic stress component, these differences are not significant here because the stress state in the adhesive is predominantly shear. Differences in predicted stress and strain levels will however be expected in

those regions of the joint where there is a significant hydrostatic stress component ie in regions of strain concentration at the ends of the adhesive layer (see section 7.2). Allowing some plastic deformation of the steel adherends is seen to have a small influence on the behaviour of the joint, but the flow stress seems to be unaffected.

4.2 A DYNAMIC ANALYSIS

A dynamic analysis allows rate-dependent materials behaviour to be included in the calculations as well as the contribution from inertial forces when the deformation speed is sufficiently high. In Abaqus, a dynamic analysis can be carried out using the standard (implicit) solver code or an explicit code. The advantage of using the standard solver is that the time step between solutions can be substantially longer than that required by the explicit solver. This means that computer processing times are significantly shorter especially at the lower loading rates. With the explicit solver, the time step is determined by the time for a stress wave to cross the smallest element dimension. This is not a problem when analyses at high loading rates are undertaken but, as noted above, processing times can be excessive at lower speeds although these can be reduced by adopting artificially high values for material densities. The main advantage of using the explicit solver is that solutions can be obtained at larger extensions than with the standard code. This is illustrated in figure 5 which compares force/extension curves for the static analysis with dynamic analyses using both solver codes. A single hardening curve and the linear Drucker-Prager model were used for the adhesive for each analysis. The adherends were assumed to be linear elastic. It is apparent that with the standard dynamic analysis, the solver failed to converge at a smaller extension than was achieved with the static analysis (see figure 4). However, the explicit solver continued to obtain solutions to substantially higher extensions.

The explicit solver therefore is particularly useful for analysing bonded joints made with very tough adhesives that sustain large extensions before failure, such as the epoxy adhesive LMD 1142 studied here. The main disadvantage at present is that the exponent Drucker-Prager model, which has been shown in previous work (2) to most closely describe yielding in this adhesive, has not been implemented in Abaqus with the explicit code. Predictions of rate dependent behaviour of the

adhesive joint specimen and performance under impact have therefore been made using the explicit code and the linear Drucker-Prager model. These analyses are considered in the next section. The exponent Drucker-Prager model and the standard solver code have however been used to predict strain distributions in the joint at extension levels in the region of 0.1 mm. These solutions are compared with results obtained using the linear Drucker-Prager model with both the standard and explicit codes and are discussed in section 7.2.

4.3 ANALYSIS WITH RATE-DEPENDENT ADHESIVE PROPERTIES

Rate-dependent plasticity is implemented in dynamic codes in Abaqus by inputting data for the strain hardening function over a range of strain rate. These data are obtained from tensile tests on bulk specimens carried out over a wide range of tensile strain rate and are shown in figure 2. The maximum strain rate achieved in these tests was 115 s^{1} which was somewhat below the levels achieved in some of the joint specimen tests. Strain hardening curves were therefore obtained out to 2500 s^{-1} by extrapolation of the data in figure 2. This was achieved by linear extrapolation of yield stress vs log strain rate plots at selected values for plastic strain. The rate-dependent hardening data used for FE simulations of joint performance at different loading speeds are shown in figure 6. The dynamic analysis in Abaqus assigns the lowest curve to a strain rate of zero. The three curves at the highest rates were obtained by extrapolation as referred to above.

As noted in section 4.2, use of the explicit solver code can give rise to long computation times when the loading speed is moderate or slow (<1 m/s). The effect of artificially raising the densities of the adhesive and adherends to reduce computation time is illustrated in figure 7. This shows force extension curves for the joint specimen obtained with the explicit solver code and the linear Drucker-Prager model at a speed of 0.1 ms^{-1}. Raising the density by factors of 10^3, 10^4 and 10^5 introduced a cycle in the force level that increases with density and is presumably associated with multiple reflections of a stress wave pulse in the specimen (see section 4.4). Using a density value raised by a factor of 100 however produced no trace of a cycle. From these results, it was concluded that carefully selected density values could be used at lower speeds without introducing inertial contributions to the predicted force. The density values selected were raised by a factor of

100 for each factor of 10 reduction in the speed of loading below 1 m/s. The computation time to a particular extension then remained constant for every test speed.

Calculated force/extension curves are shown in figure 8 for loading speeds equal to and below 0.1 m/s. At these speeds, inertial forces are negligible and the load was applied using displacement control. Comparisons with experimental data are also shown in figure 8 and are discussed in section 7.1. At higher speeds, contributions to the force record arise through the excitation of shock waves and resonances in the test arrangement. These are considered in section 4.4.

4.4 ANALYSIS OF TRANSIENT FORCES GENERATED BY AN IMPACT

Calculated force/extension curves at speeds of 1 m/s and above are shown in figures 9 and 10. These were obtained under velocity control. Figure 9 considers an impact velocity of 1 m/s and shows the predicted response obtained for the lap joint in series with a spring representing the stiffness of the force transducer. A mass of 170 g is located between the specimen and the spring to represent the mass of the transducer attachment and the specimen support (see figure 11). The force/extension record obtained when the transducer is assumed to have infinite stiffness is similar to the curves shown in figure 8 but has superimposed on it an oscillatory force of period about 2.5×10^{-5}s. This is approximately the time taken for an acoustic pulse to travel the length of the specimen and back. The oscillations can therefore be explained as multiple reflections of a shock wave pulse excited by the impact of the falling weight on the end of the specimen. This interpretation is supported by calculations obtained for a specimen of twice the length for which the oscillation period doubled in value.

The second trace in figure 9 was obtained when the force transducer stiffness was assigned the value 430 kN/mm. Here, the high frequency oscillation is absent and is replaced by a lower frequency vibration of around 8 kHz. This is caused by a resonance of the force transducer acting as a simple spring with a suspended mass. The amplitude of the vibration will be related to the magnitude of the impulse force to which the specimen was subjected by the falling weight. The slower rise time of the force when the transducer has a finite stiffness is presumably due to the time required to accelerate

the mass attached to the force transducer. The absence of any sign of multiple reflections of the stress wave pulse for this situation may be caused by attenuation of the reflected wave amplitude when one boundary of the specimen has some compliance.

In figure 10, predicted force/extension curves are shown for impactor velocities of 2 m/s and 4.4 m/s with the force transducer represented as a spring and mass as considered in figure 9. The force record is now dominated by the transducer resonance which lies at a frequency of 8 kHz independent of the impact velocity. The amplitude of the resonant vibration increases with the velocity of impact by virtue of the increase in the impulse force which is proportional to the change in momentum of the end of the specimen struck by the falling weight. Experimental data are also shown in figure 10, and comparisons with the FE results are discussed in section 7.3.

5 EXPERIMENTAL TESTS ON JOINT SPECIMENS

Impact tests on joint specimens have been carried out using the falling weight apparatus shown in figure 11. The specimen is loaded by means of pins that pass through holes located near the ends of each adherend. Each pin is held by a support. The upper support is bolted to a piezoelectric force transducer that is suspended from a rigid frame. The lower pin support is attached to an anvil that is struck by the falling mass. The specimen is a close fit in the aperture in the pin supports, and the aperture is displaced laterally from the axis of the loading assembly so that the adhesive layer coincides with this axis. The force on the specimen is measured at discrete times throughout the impact, and a force vs extension plot is derived from the force vs time record by integration. The extension values will contain contributions arising from the compliance of the test assembly and the pin-loading supports. A correction to these values has not been applied but could be derived from separate measurements of apparatus compliance.

Results of impact tests at speeds of 2 and 4.4 m/s on lap-joint specimens of the epoxy adhesive are compared with predictions in figure 10. The curves shown are typical results of tests that were carried out on 3 sets of test specimens.

In order to aid the interpretation of these impact data, tests have also been carried out under controlled displacement rate in a servohydraulic test machine. For this purpose, the specimen supports and load cell were removed from the falling-weight impact test and mounted in the loading assembly of the servohydraulic machine. For test speeds of 0.1 m/s and slower, the extension of the joint was measured using extensometers attached to the wide faces of the adherends and having a gauge length of 25 mm. Two extensometers were used to improve measurement accuracy. A series of force vs extension curves obtained at different test speeds is compared with predicted curves in figure 8. These curves are again typical of results obtained on several sets of test specimens. In these tests, the acceleration of the actuator to reach the set speed is achieved within a displacement of 0.1 mm. The remainder of the test is then carried out under constant speed.

6 A FAILURE CRITERION

A criterion for ductile failure of the adhesive under short-term monotonic loading has been proposed (1) based on attaining a critical level of strain. Earlier work involving the use of butt-torsion tests (3) revealed that large shear strains can be developed in adhesives without failure. This indicates that, if a critical strain criterion for failure is valid, it is the hydrostatic (volumetric) component that primarily determines the critical value. Analysis of the results of failure tests on bulk and butt-joint specimens in tension reveal that a critical level of hydrostatic strain is not a sufficient criterion. This implies that whilst a significant hydrostatic strain must be present to initiate failure, the critical level is dependent upon the magnitude of the associated shear component. This is illustrated in figure 12 which shows failure strains obtained from tensile tests on bulk and butt-joint specimens plotted on axes of I_1 vs $I_{2D}^{1/2}$. I_1 and $I_{2D}^{1/2}$ are the hydrostatic and deviatoric strain components in the adhesive at failure and are related as follows to true principal strain components ε_1^f, ε_2^f and ε_3^f at failure which are measured in the tests.

$$I_1 = \varepsilon_1^f + \varepsilon_2^f + \varepsilon_3^f \qquad (6)$$

$$I_{2D}^{1/2} = \left\{\frac{1}{6}\left[(\varepsilon_1^f - \varepsilon_2^f)^2 + (\varepsilon_2^f - \varepsilon_3^f)^2 + (\varepsilon_3^f - \varepsilon_1^f)^2\right]\right\}^{1/2} \quad (7)$$

The failure data lie on the empirical curve

$$I_1 = A \exp - B\, I_{2D} \quad (8)$$

where A = 0.17 and B = 66 are material parameters that will depend upon temperature and strain rate. The failure criterion

$$\ln \frac{I_1}{A} + B\, I_{2D} \geq 0 \quad (9)$$

follows from equation 8.

7 COMPARISON OF PREDICTED AND MEASURED JOINT PERFORMANCE

7.1 COMPARISON OF RESULTS AT LOW SPEEDS

Predicted and measured force/extension curves for the lap-joint specimen obtained at low deformation speeds are compared in figure 8. The extension at failure is about 0.5 mm implying a mean shear strain in the adhesive at failure of around 100%.

It is a apparent from figure 8 that, at low extensions (<0.1 mm) where the deformation behaviour of the adhesive is linear, the predicted force/extension curve coincides with measured values. However, at larger strains, the predicted curve at each loading speed departs from measured data, and the predicted maximum stress is consistently higher than measured values. Despite this, the observed increase in the flow stress with increasing loading speed is reliably simulated. It was conceivable that the joint specimens, having cured in a specimen preparation jig, had not reached

recommended cure temperature for a sufficient time period to effect complete cure. Repeat tests were therefore performed on joint specimens for which the cure time at elevated temperature had been extended. No significant change in the results of tests on these specimens, were however, observed.

An alternative explanation was considered whereby the adhesive is failing locally at an extension just below 0.1 mm which is where the measured and predicted curves depart in figure 8. This will lead to a reduction in the amount of adhesive that is able to sustain load and thus an increase in the stress level in the remainder of the adhesive. The adhesive will therefore reach the flow stress appropriate to each strain rate at a lower force than predicted for the undamaged bond. One possibly surprising implication of this interpretation is that, despite the local failure of the adhesive at low extensions, the layer is capable of sustaining substantially higher extensions before complete failure.

7.2 EVALUATION OF STRAIN DISTRIBUTIONS

7.2.1 The onset of failure

In order to explore this interpretation further, finite element calculations were made of the strain distribution in the adhesive. Contours of maximum principal strain at an extension of 0.1 mm are shown in figure 13. These results were obtained using the explicit solver, the linear Drucker-Prager materials model and a loading speed of 0.1 m/s. Rate-dependent hardening data were used. A region of strain concentration is located at the end of the radius at the end of each adherend. The peak value for the maximum principal strain in this region is about 6%. The strain analysis also revealed that the other principal strain components in this region were 0 (arising from the assumption of plane strain in the specimen) and -3.5%. From these values, the magnitudes of the strain invariants I_1 and $I_{2D}^{1/2}$ were calculated at the position of maximum strain using equations (6) and (7). Comparison of these values with the failure criterion introduced in section 6 and illustrated for this adhesive in figure 12 reveals that the calculated strain level in the adhesive at 0.1 mm extension is well below the strain at which any rupture of the adhesive is expected to occur.

It should be noted that these strain predictions were obtained using the linear Drucker-Prager materials model which has been shown in previous work (2) to be less appropriate for this adhesive than the exponent version. Some error in the calculated strain values is therefore expected. The exponent Drucker-Prager model has not yet been implemented in Abaqus with the explicit solver. A dynamic analysis was therefore attempted using the standard solver. However with the rate-dependent hardening data (figure 6), the analysis failed to converge at even earlier extensions than that shown in figure 5. To explore the nature of strain solutions obtained with the exponent Drucker Prager model, a static analysis was therefore carried out using hardening data at a single strain rate. Hardening data at the strain rate of 115 s^{-1} were selected from figure 6 since this rate is close to the mean strain rate in the adhesive at a loading speed of 0.1 m/s. The static analysis using the exponent Drucker-Prager model then gave a similar strain map and peak strain (5.8%) at an extension of 0.1 mm to that obtained with the linear Drucker-Prager model and the explicit solver.

We conclude that the departure of measured and predicted force/extension curves at an extension of 0.1 mm cannot be reliably explained by the initiation of a local failure of the adhesive since the strain levels are too low. The reason for the discrepancy between measured and predicted behaviour therefore remains unclear and must be a subject for further work.

7.2.2 Further strain analyses

The predicted force/extension curves in figure 8 reach a maximum force level at an extension of around 0.2 mm after which the force is essentially constant. The measured curves peak at extensions between 0.2 and 0.3 mm after which the force shows a slow decrease with further extension. These observations are another indication that local and progressive failure is occurring in the adhesive, initiating presumably in the region of strain concentration.

In order to explore further the scope for using strain calculations to predict the onset of failure in adhesive joints, the results of strain analyses were obtained at extensions beyond 0.1 mm. In these analyses, the influence of the choice of the materials model on strain predictions has been

investigated further. In addition, comparisons are made between strain levels calculated using the quasi-static analysis (single rate hardening function) and a dynamic analysis with rate-dependent hardening data. The influence of allowing plastic deformation in the steel adherends is also explored.

Strain distributions in the adhesive have been calculated out to an extension of 0.2 mm. The peak value of the maximum principal strain (located in the region of strain concentration in figure 13) was derived at discrete extensions, and results from different analyses are shown in figure 14. Figure 14a compares principal strains obtained using a quasi-static analysis with the linear and exponent Drucker-Prager models. A single hardening curve at the strain rate of 115 s^{-1} was employed. It is apparent that the solutions using the two models start to differ at extensions above 0.1 mm, the exponent Drucker-Prager model giving higher strains.

Figure 14b compares principal strains obtained using the linear Drucker-Prager model and the quasi-static analysis with results from a dynamic analysis using the explicit solver and rate-dependent hardening data. The static analysis gives higher strain values which may be due to the need with the static analysis to select a hardening curve for a single strain rate. The rate chosen (115 s^{-1}) may be too low for the actual strain rate in the region of peak strain in the adhesive at 0.1 m/s.

Figure 14c shows the influence of allowing plastic deformation to occur in the steel adherend. The linear Drucker-Prager model was used with the explicit solver. At extensions above 0.1 mm, the analysis with steel plasticity gives significantly lower strain levels than the case where only linear elastic behaviour of the steel is considered. This analysis with steel plasticity probably gives the most accurate of the strain predictions shown in figure 14. These results will now be used to calculate the strain state at an extension of 0.2 mm where, from figure 8, there are indications that local, non catastrophic rupture of the adhesive layer is starting.

The calculated value of the maximum principal strain in the region of strain concentration in the adhesive at an extension of 0.2 mm is 0.18, from figure 14c. From the FE calculation, the other principal strain components in this region and at the same extension are zero (plane strain assumption) and -0.09. From equations (6) and (7), the strain invariants I_1 and $I_{2D}^{1/2}$ in the region of peak strain then take values

$$I_1 = 0.09$$

and $$I_{2D}^{1/2} = 0.14$$

This strain state is just outside the failure envelope for the adhesive shown in figure 12 implying that failure initiation would be expected at a slightly smaller extension than 0.2 mm. This result gives support to the application of the proposed failure criterion (section 6) for predicting the onset of local failure in a bonded joint. Also, there is scope for refining the strain analysis further by use of a more realistic materials model, the inclusion of rate-dependence in the failure criterion and, possibly, use of a 3-dimensional analysis.

7.3 COMPARISON OF RESULTS AT IMPACT SPEEDS

Comparisons of measured and predicted performance of joint specimens under impact loading are made in figure 10 which shows force/extension curves at impact speeds of 2 and 4.4 m/s. As noted in section 4.4, the predicted response is dominated by the excitation of a resonance of the force transducer whose amplitude is determined by the magnitude of the impulse force generated by the impact. The experimental curves show essentially the same phenomenon. At 2 m/s, the experimental record shows evidence of transducer resonance at a frequency close to 8 kHz but which is attenuated and distorted, presumably because of sources of damping that have not been included in the analysis. Also, the height of the first peak is lower than predicted for both the 2 and 4.4 m/s traces. Some compliance of the test assembly or of the striker/anvil interface would reduce the impulse force and hence the height of the first peak and of the subsequence resonance amplitude. The mean force level under flow for the measured trace at 2 m/s is slightly below the predicted trace, and this is consistent with the results at lower speeds shown in figure 8 and discussed in section 7.1. At 4.4 m/s, the experimental results show evidence of specimen failure near the first minimum of the resonance. As noted in section 5, the experimental impact results were not corrected for compliance of the test assembly. Deformation of the assembly during impact will therefore contribute to the derived extension values, and this explains why the measured curves in figure 10 appear displaced along the extension axis in comparison with the calculated curves.

8 CONCLUDING REMARKS

Finite element methods can be used to predict the force/extension curves of joint test specimens loaded at different speeds. With toughened adhesives, an elastic-plastic materials model is needed, and, for increased accuracy, this model should employ a yield criterion with sensitivity to the hydrostatic component of stress. The materials parameters for these models can be derived from tensile and shear tests on bulk specimens of the adhesive. Rate-dependent behaviour is included in the analysis by supplying strain hardening curves over a range of strain rate obtained from tensile tests carried out at different loading speeds.

Problems with convergence of the analysis have been experienced when using a dynamic analysis with the standard solver code. These problems limit the extension of the joint specimen at which solutions can be obtained but can be avoided by using the explicit solver whereby solutions can then be obtained out to relatively large extensions.

When loading speeds exceed about 1 m/s, such as in impact tests, transient forces are superimposed on the force/extension curve. Finite element analyses have shown how these can arise through multiple reflections of shock waves, generated by the impact, and by a resonance of the force transducer acting as a spring in series with the specimen.

With the Ciba adhesive studied here, calculated force/extension curves coincided with measured results in the linear elastic region of the adhesive only. At higher extensions, where plastic deformation of the adhesive occurs, predicted forces were consistently higher than measured forces. Attempts to explain this in terms of local rupture of the adhesive at regions of strain concentration have not been successful. The maximum strain in the adhesive at the extension where measured and predicted force/extension curves start to depart is well below the strain level where rupture of the adhesive is feasible. The only explanation that can currently be proposed is that adhesive property values derived from bulk specimens and used to predict joint performance are not representative of

the adhesive material in a bonded joint. This conflicts with earlier studies (4) that demonstrated that bulk and joint test specimens for a variety of adhesives had similar properties. However, this Ciba adhesive has an unusual morphology which gives the material exceptional toughness, but the microstructure may be sensitive to the conditions under which the cured adhesive is prepared. Investigations similar to those reported here are planned on other adhesive materials.

Further comparison of measured and predicted force/extension curves indicate that local rupture of the adhesive may be initiated at an extension in the region of 0.2 mm. Calculations of the strain level and state at this extension at the location of peak strain in the adhesive are consistent with the failure criterion described in section 6. This result gives support to the use of a failure criterion based on a critical state of strain in the adhesive as a method for predicting failure or the onset of failure in a bonded joint. To establish more confidence in this approach to failure predictions, further work is needed on other types of adhesive and joint geometries.

ACKNOWLEDGEMENTS

This work was funded by the Department of Trade and Industry as part of The Performance of Adhesive Joints programme. The assistance of Mr A Pearce by carrying out the tests on joint specimens is also acknowledged.

REFERENCES

1. G. Dean and L. Crocker, A proposed failure criterion for tough adhesives. NPL Report CMMT(A)158, February 1999.

2. G. Dean, B. Read and B. Duncan, An evaluation of yield criteria for adhesives for finite element analysis. NPL Report CMMT(A)117, January 1999.

3. R. Thomas and R. Adams, Test methods for determining shear property data for adhesives suitable for design. Part 2: The torsion method for bulk and joint test specimens, April 1996. Report No 7 of Project 1 of the DTI funded programme on the Performance of Adhesive Joints, 1993-1996.

4. G. Dean, B. Duncan, R. Adams, R. Thomas and L. Vaughn, Comparison of bulk and joint specimen tests for determining the shear properties of adhesives, April 1996. Report No 9 of Project 1 of the DTI funded programme on the Performance of Adhesive Joints, 1993-1996.

FIGURE CAPTIONS

Figure 1 Schematic diagram of the joint test specimen.

Figure 2 Experimental values of the strain hardening function over a range of strain rates between 2.10^{-5} s^{-1} and 115 s^{-1} derived from tensile tests on bulk specimens of the adhesive.

Figure 3 The mesh used for finite element analyses of the joint test specimen.

Figure 4 Comparison of force vs extension predictions of the joint test specimen using three materials models. The extension refers to a 25 mm gauge length centred on the middle of the overlap region. A quasi-static analysis has been carried out using a hardening curve at a strain rate of 115 s^{-1}.

Figure 5 Comparison of force/extension curve predictions obtained using a dynamic analysis with the standard and explicit solvers. The linear Drucker Prager model was used with a single hardening curve obtained at a strain rate of 115 s^{-1}.

Figure 6 Hardening curves used in dynamic analysis of the joint specimen under different loading speeds. The three curves at the higher strain rates were obtained by extrapolation of data at lower rates.

Figure 7 Comparison of predicted force/extension curves at a loading speed of 0.1 m/s^{-1} for different scaling factors for the densities of the adhesive and the adherends.

Figure 8 Comparison of predicted force/extension curves for the joint specimen at different loading speeds with measurements made using controlled displacement rate tests.

Figure 9 Calculated force/extension curves illustrating the effect of the resonance of the force transducer on results.

Figure 10 Comparison of predicted force/extension curves for the joint test specimen at different test speeds with measurements obtained from falling weight impact tests.

Figure 11 Schematic diagram of the falling weight impact test used to measure the impact performance of joint test specimens.

Figure 12 Plot of strain components I_1 vs $I_{2D}^{1/2}$ (see equations 6 and 7) at failure obtained from tensile tests on bulk and butt-joint specimens of the epoxy adhesive.

Figure 13 Contours of maximum principal strain in the adhesive at an extension of 0.1 mm obtained using the linear Drucker-Prager model and a dynamic analysis with the explicit solver and rate-dependent data.

Figure 14 Peak values of the maximum principal strain against extension using different analyses. (a) comparison of results obtained with the linear and exponent Drucker-Prager materials models. (b) comparison of results using quasi-static and dynamic analyses. (c) influence of steel plasticity.

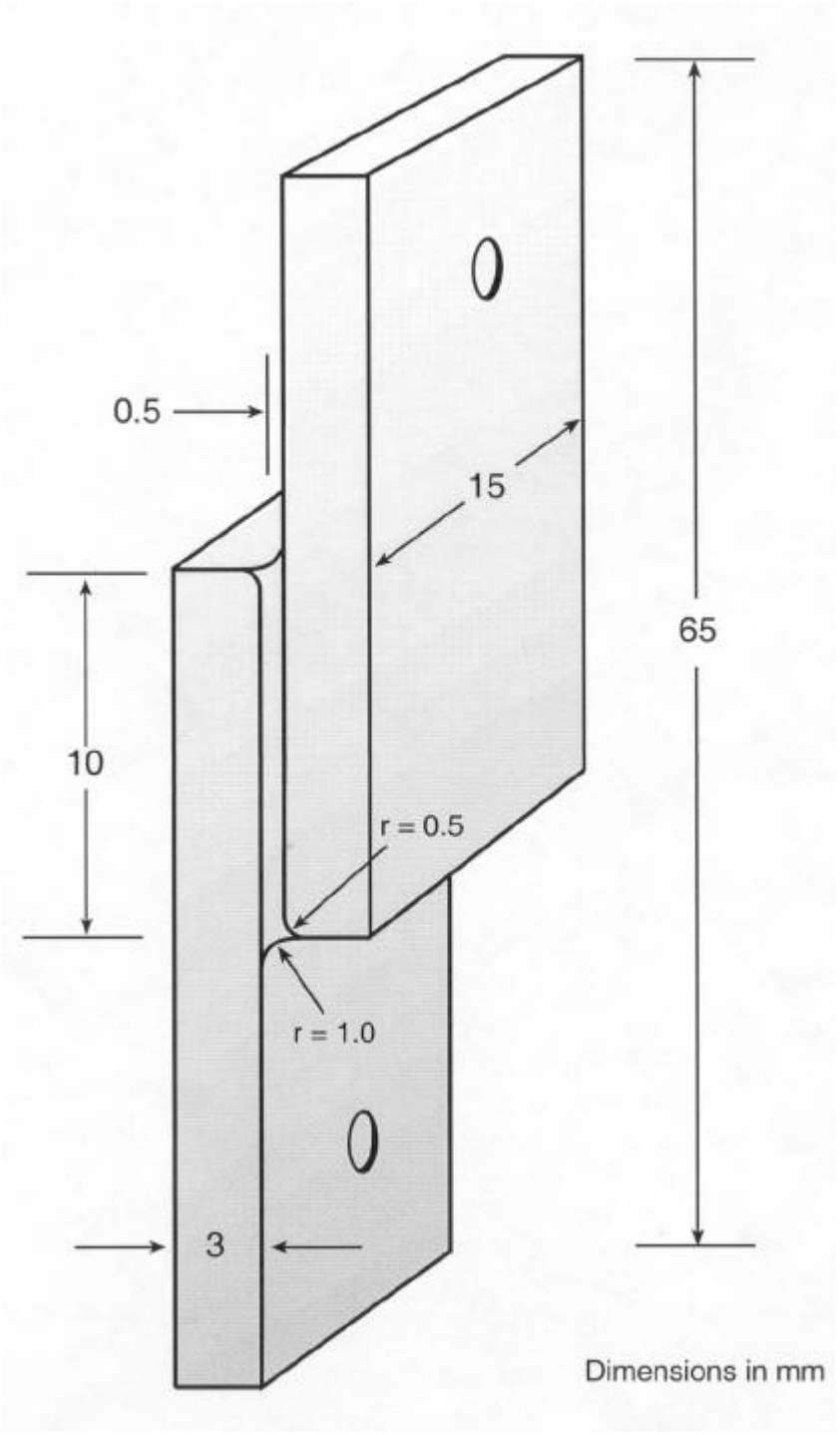

Figure 1 Schematic diagram of the joint test specimen.

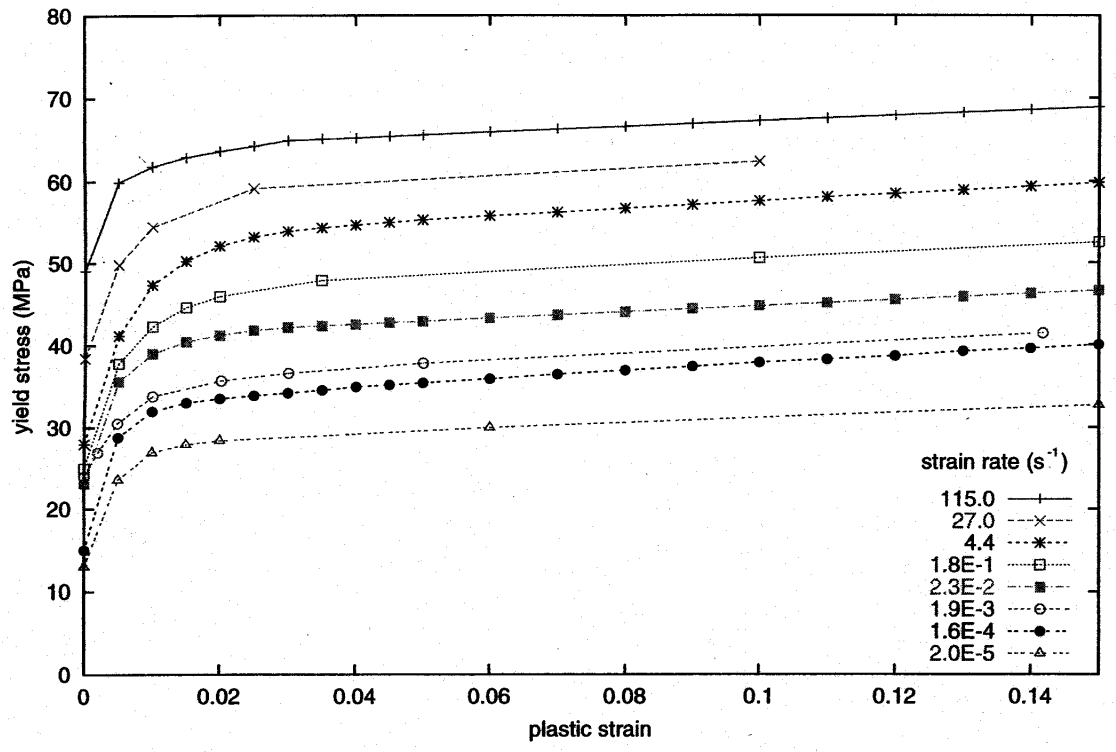

Figure 2 Experimental values of the strain hardening function over a range of strain rates between 2.10^{-5} s^{-1} and 115 s^{-1} derived from tensile tests on bulk specimens of the adhesive.

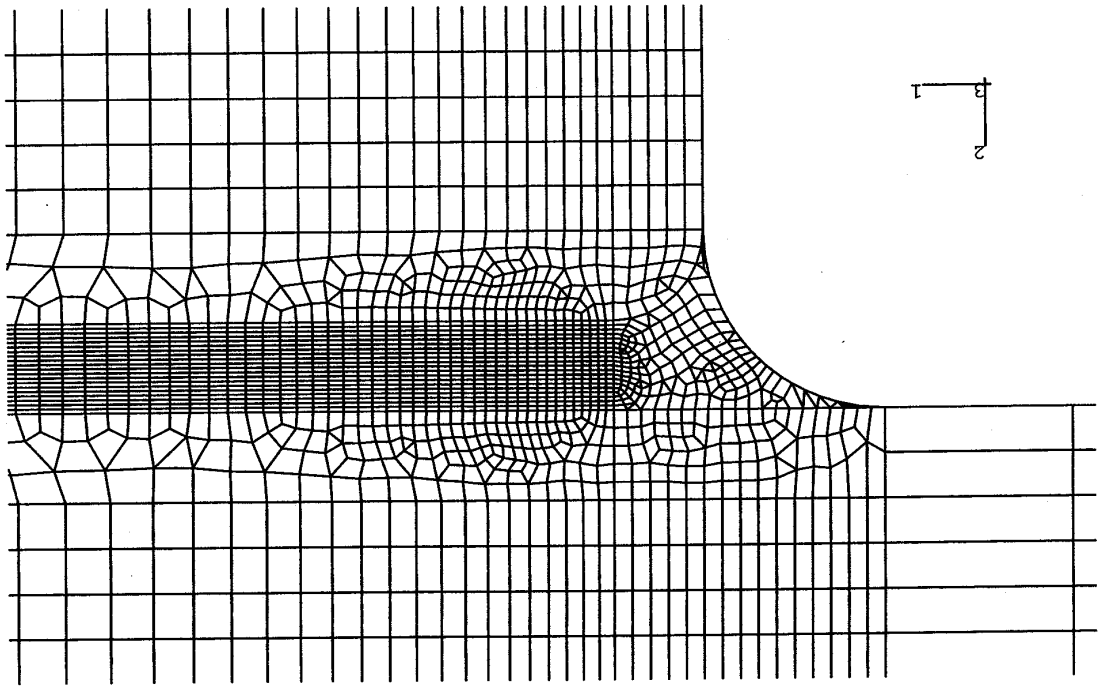

Figure 3 The mesh used for finite element analyses of the joint test specimen.

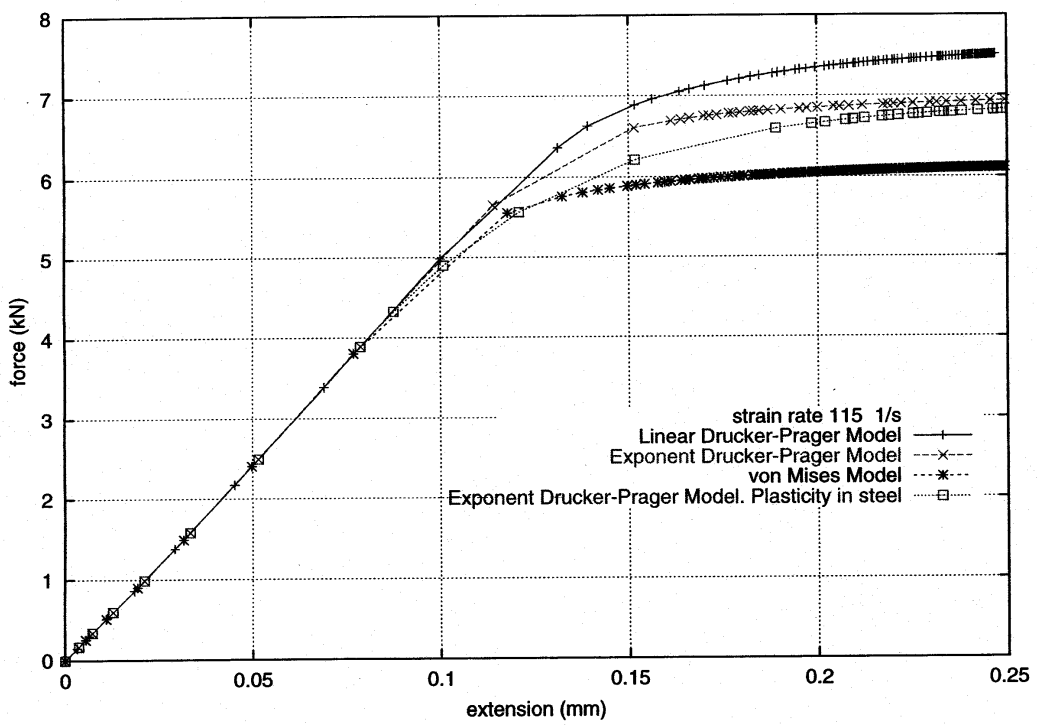

Figure 4 Comparison of force vs extension predictions of the joint test specimen using three materials models. The extension refers to a 25 mm gauge length centred on the middle of the overlap region. A quasi-static analysis has been carried out using a hardening curve at a strain rate of 115 s^{-1}.

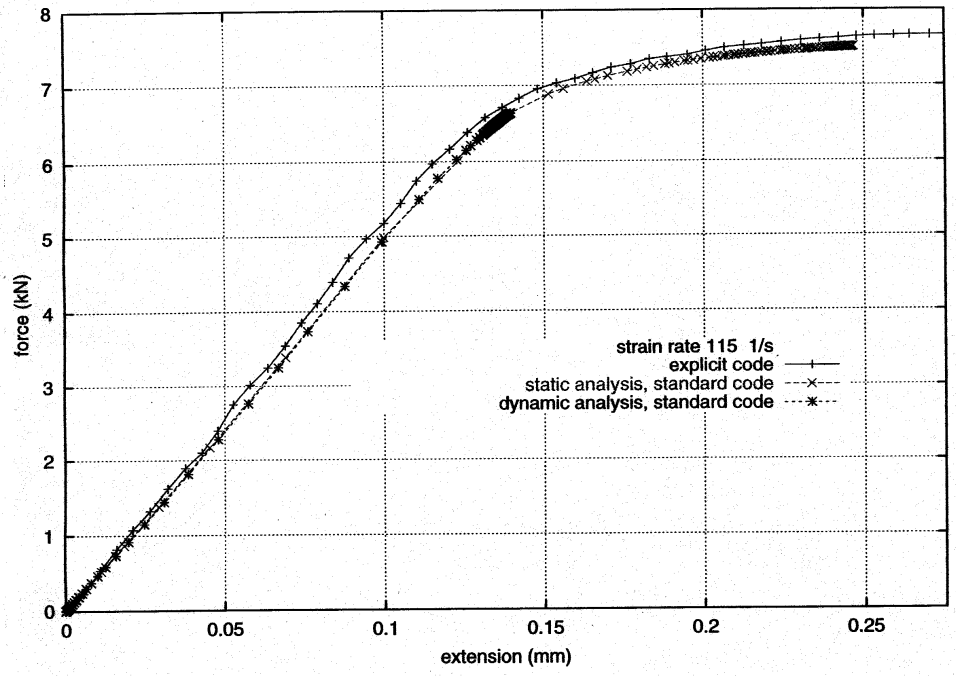

Figure 5 Comparison of force/extension curve predictions obtained using a dynamic analysis with the standard and explicit solvers. The linear Drucker Prager model was used with a single hardening curve obtained at a strain rate of 115 s^{-1}.

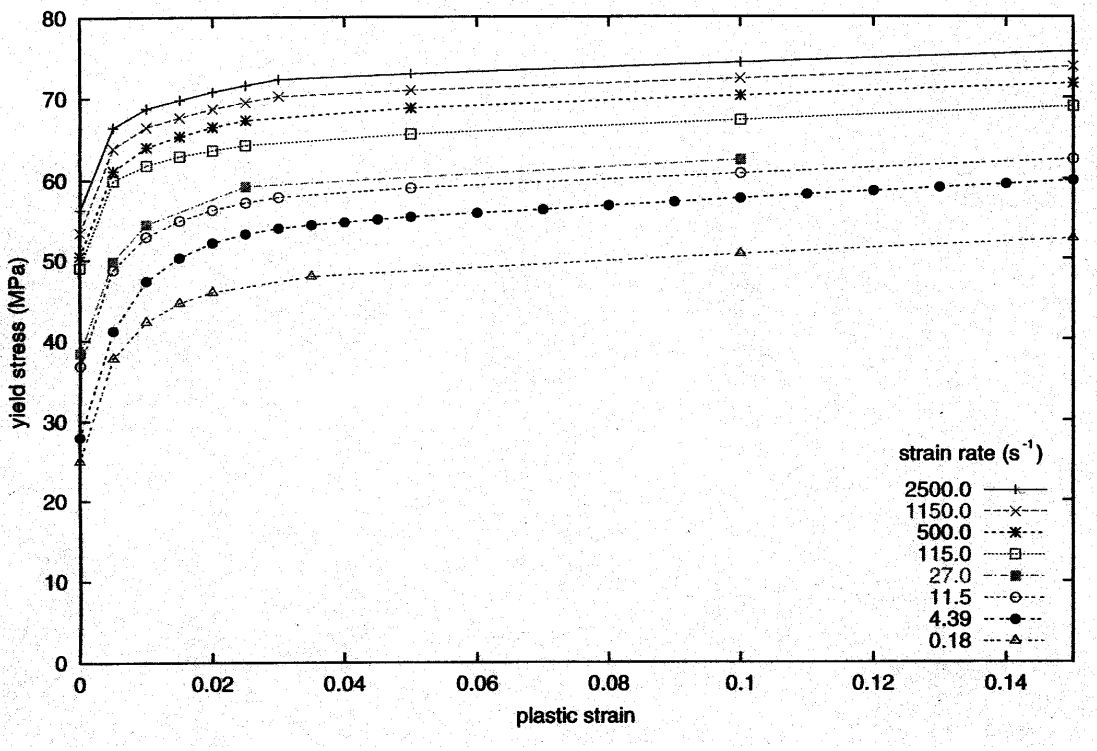

Figure 6 Hardening curves used in dynamic analysis of the joint specimen under different loading speeds. The three curves at the higher strain rates were obtained by extrapolation of data at lower rates.

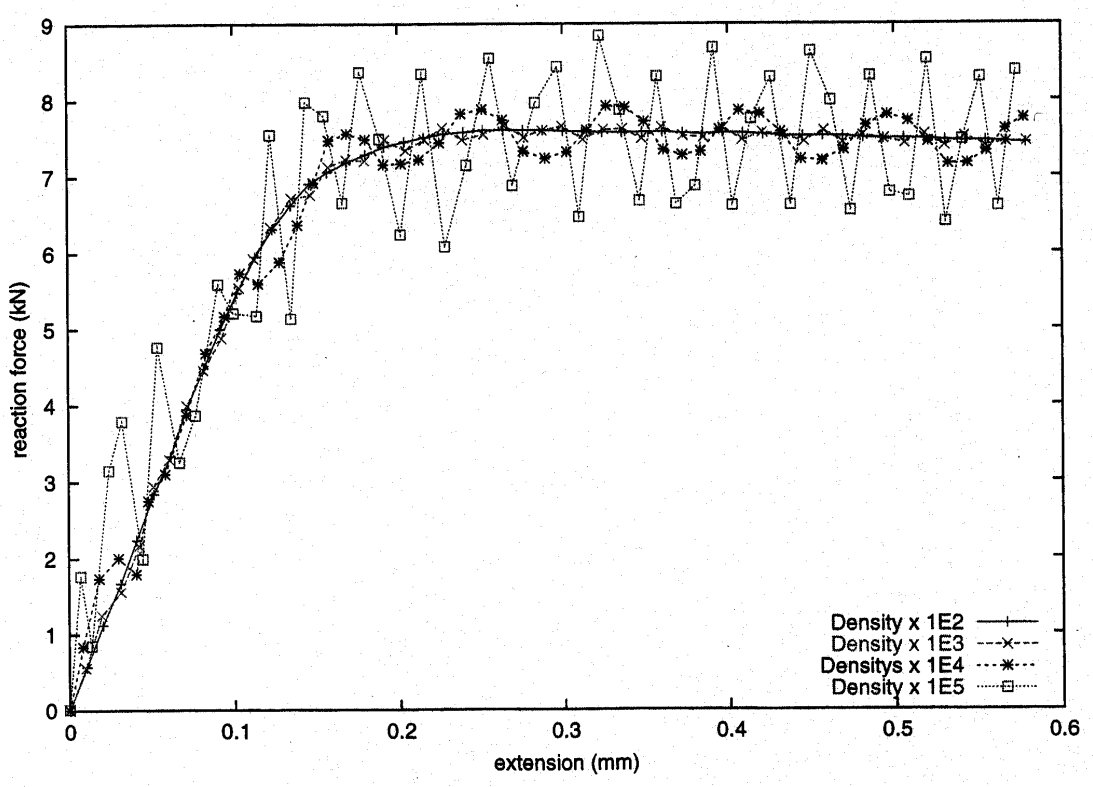

Figure 7 Comparison of predicted force/extension curves at a loading speed of 0.1 m/s^{-1} for different scaling factors for the densities of the adhesive and the adherends.

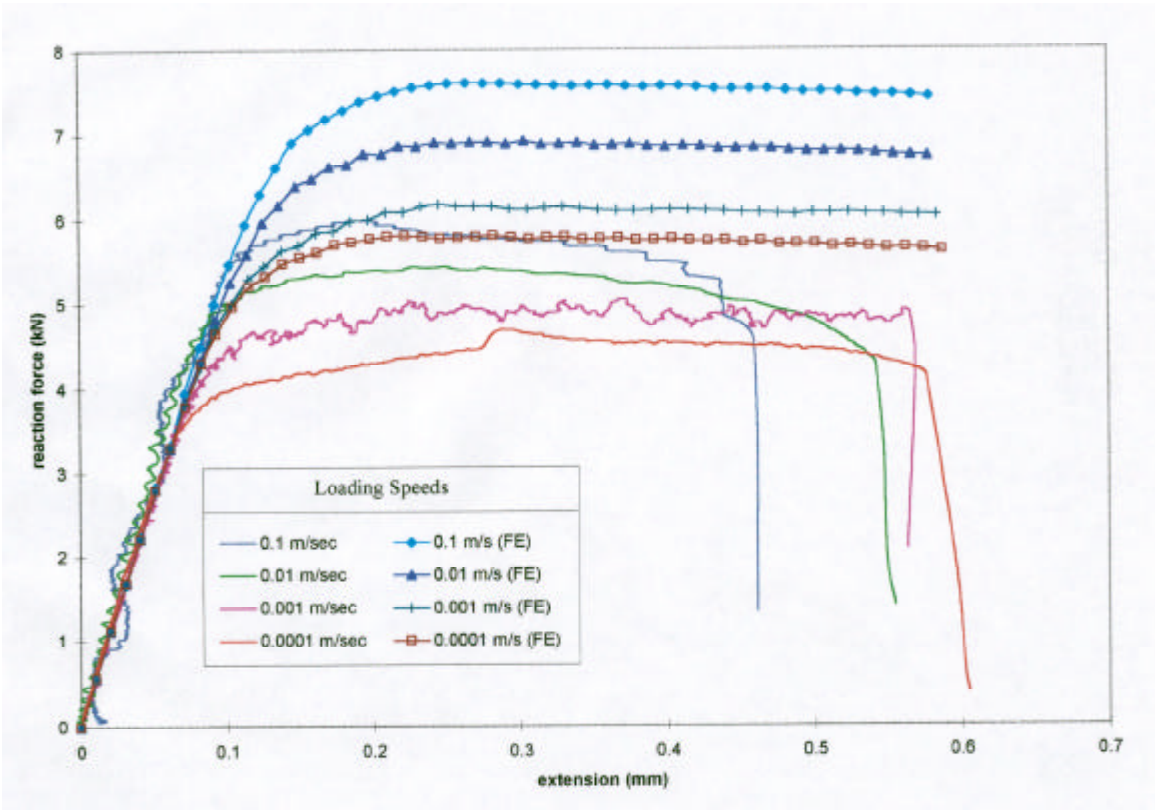

Figure 8 Comparison of predicted force/extension curves for the joint specimen at different loading speeds with measurements made using controlled displacement rate tests.

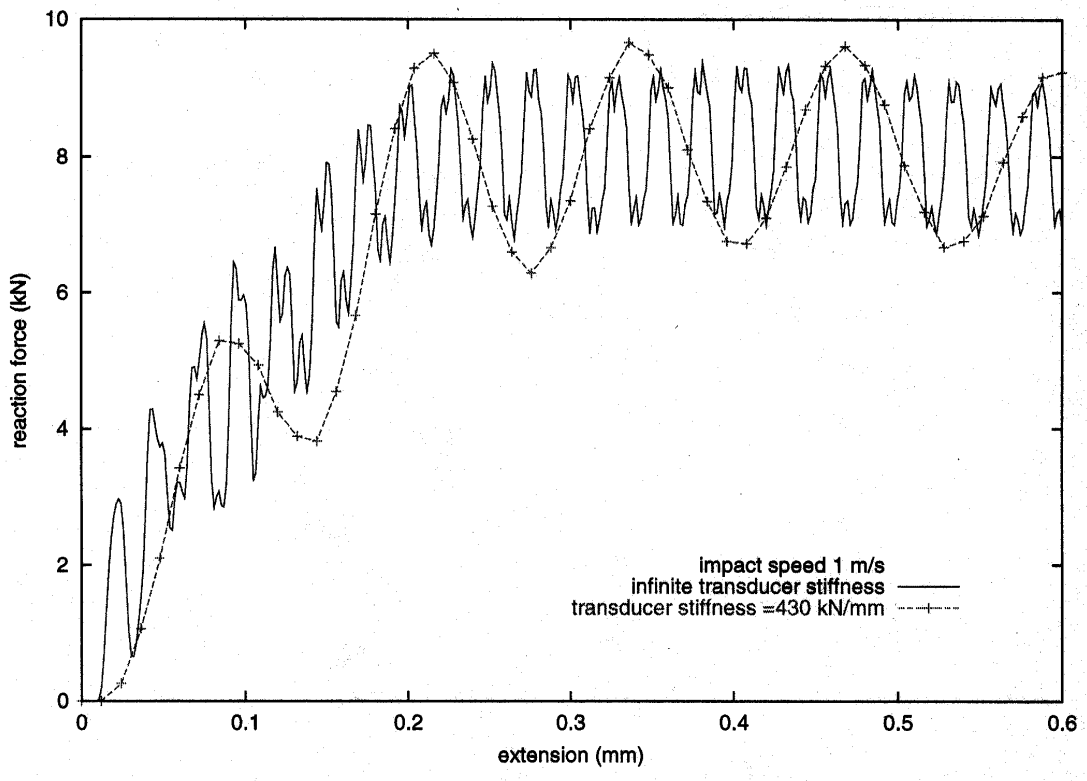

Figure 9 Calculated force/extension curves illustrating the effect of the resonance of the force transducer on results.

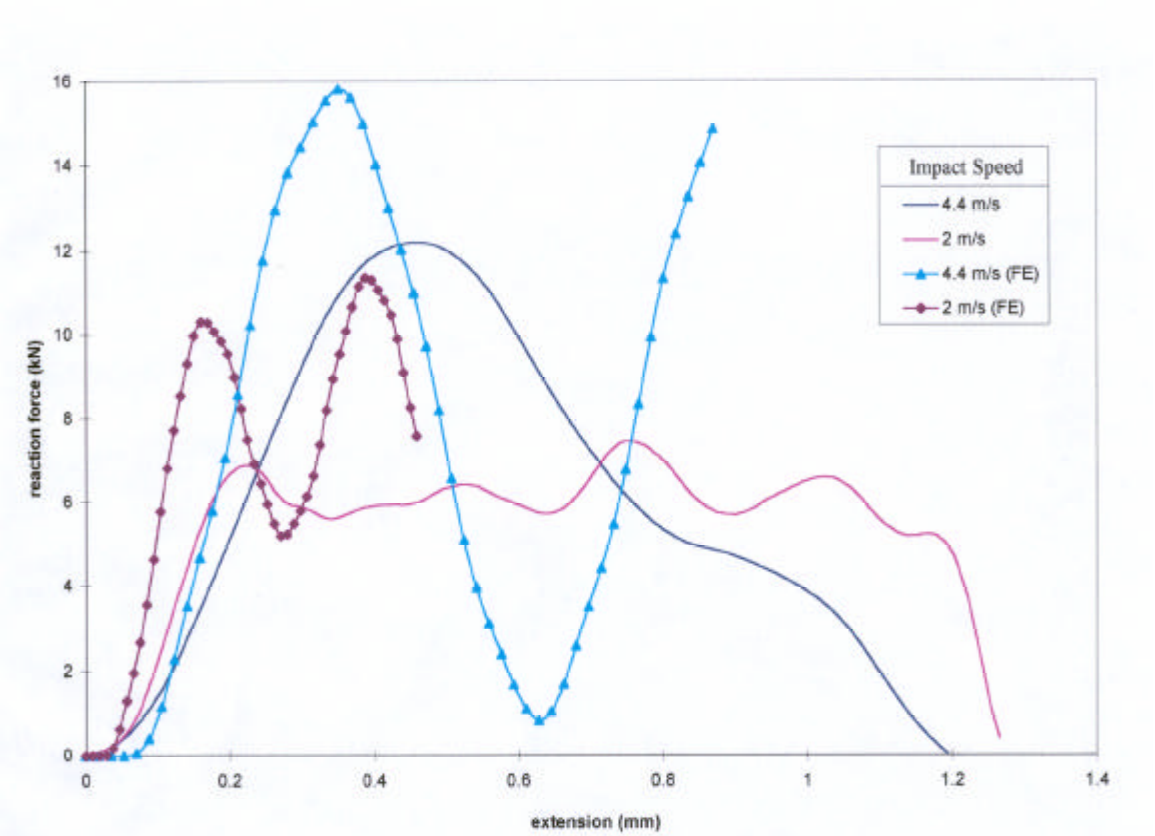

Figure 10 Comparison of predicted force/extension curves for the joint test specimen at different test speeds with measurements obtained from falling weight impact tests.

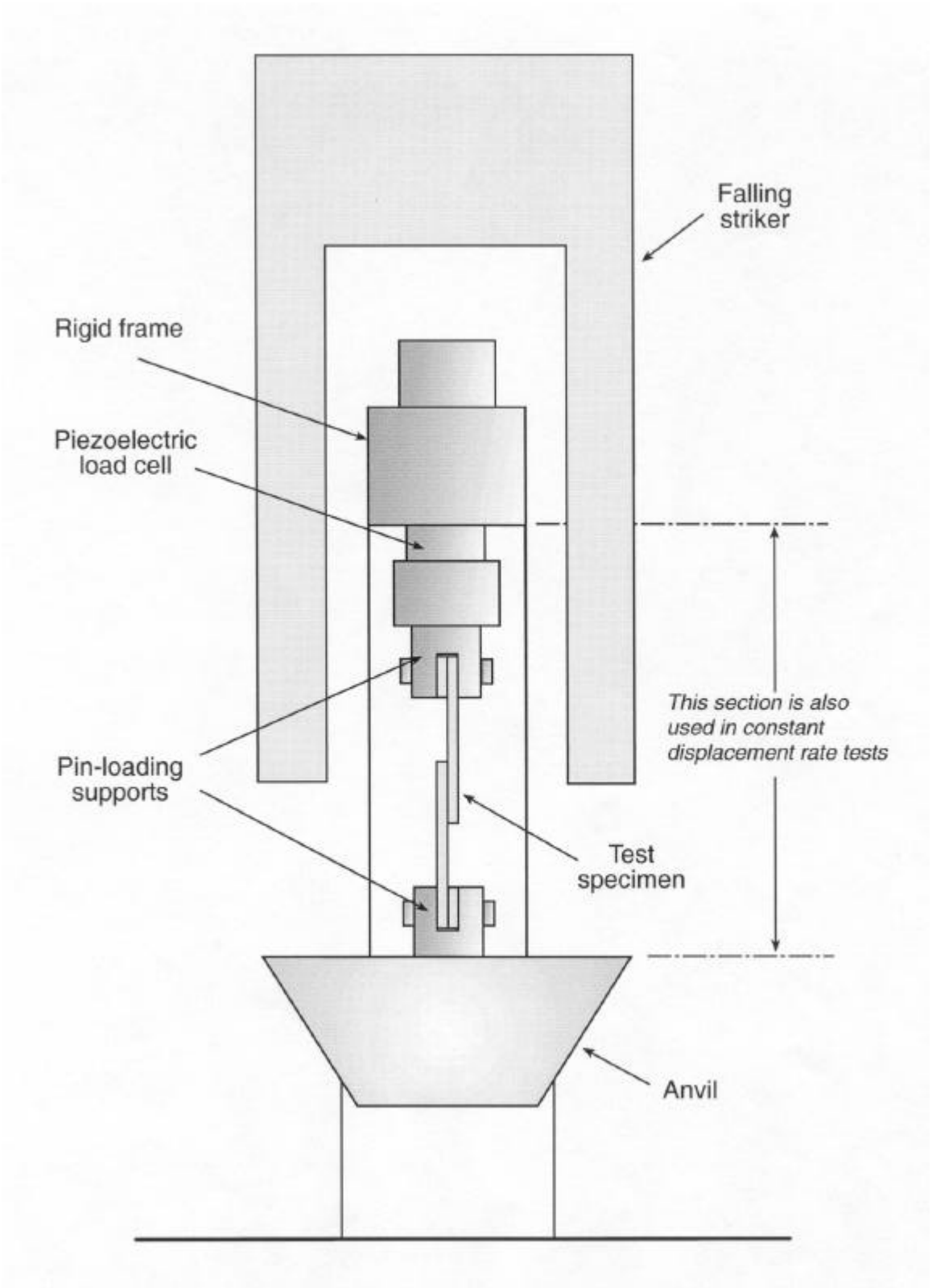

Figure 11 Schematic diagram of the falling weight impact test used to measure the impact performance of joint test specimens.

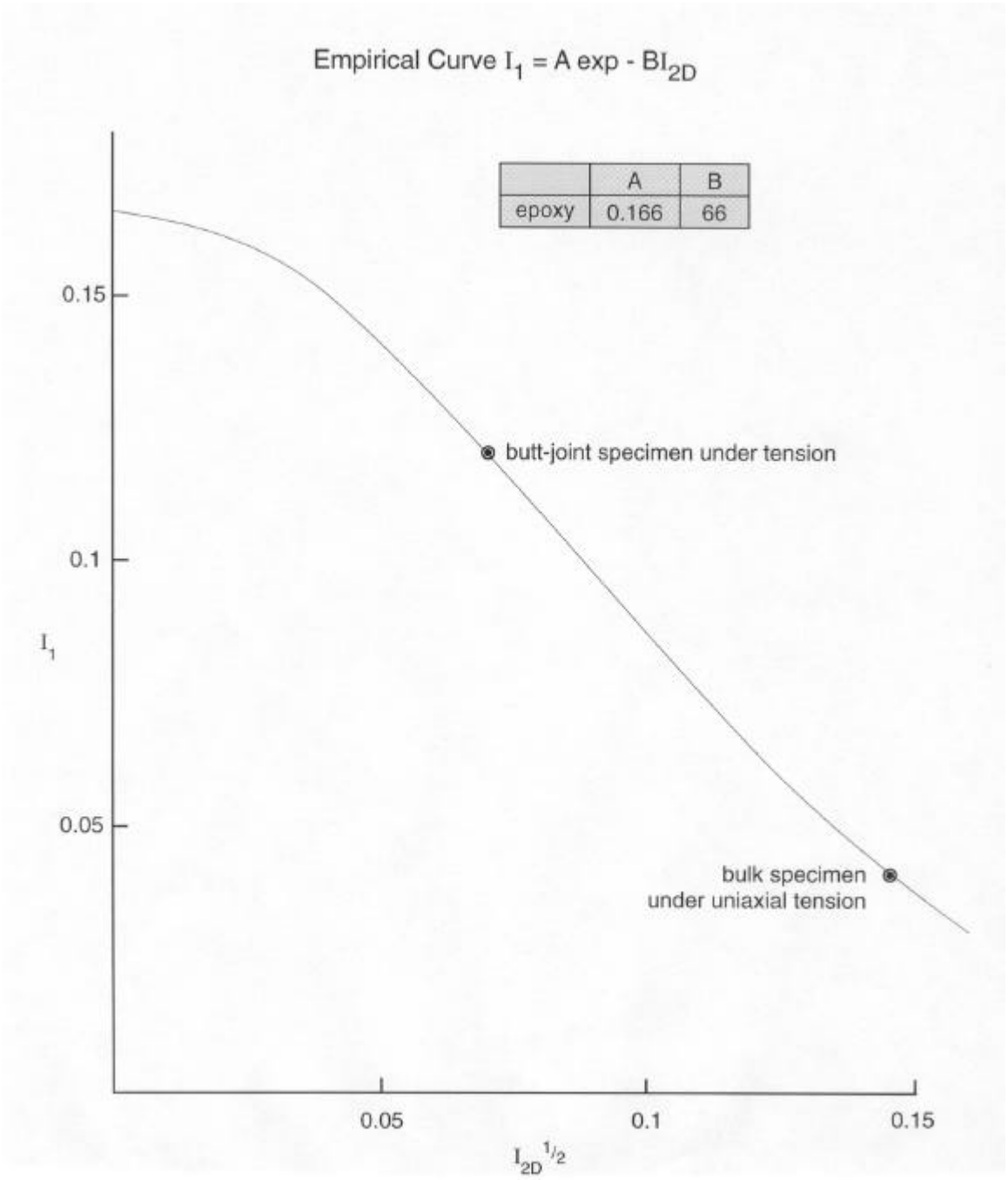

Figure 12 Plot of strain components I_1 vs $I_{2D}^{1/2}$ (see equations 6 and 7) at failure obtained from tensile tests on bulk and butt-joint specimens of the epoxy adhesive.

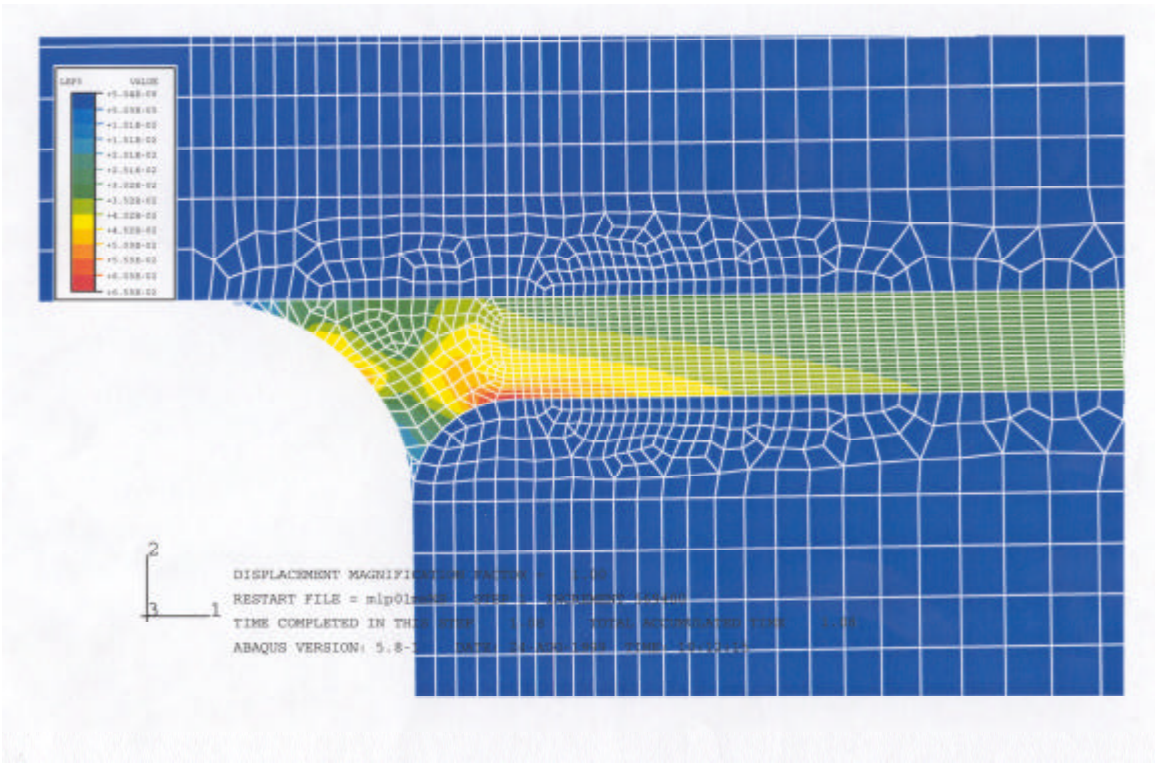

Figure 13 Contours of maximum principal strain in the adhesive at an extension of 0.1 mm obtained using the linear Drucker-Prager model and a dynamic analysis with the explicit solver and rate-dependent data.

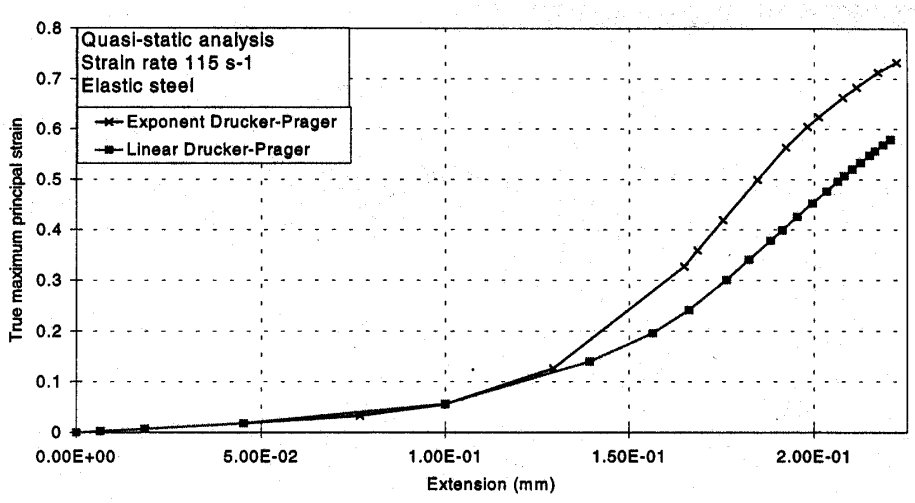

(14a)

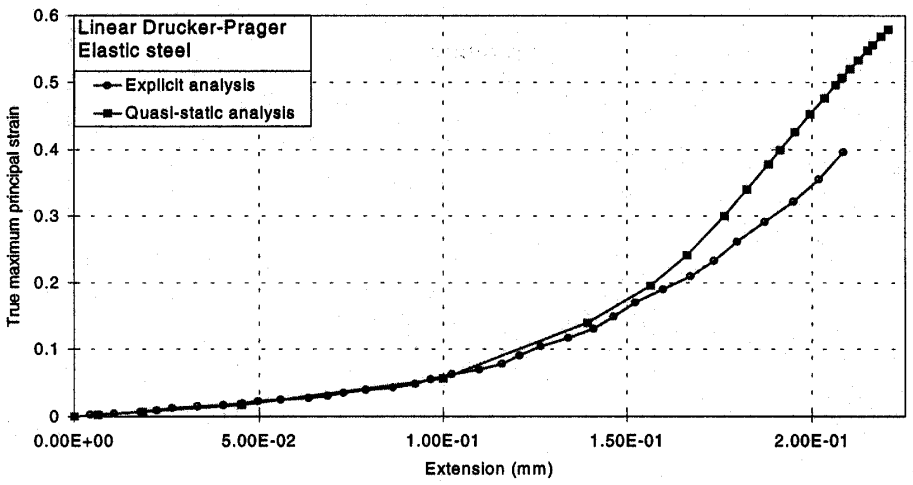

(14b)

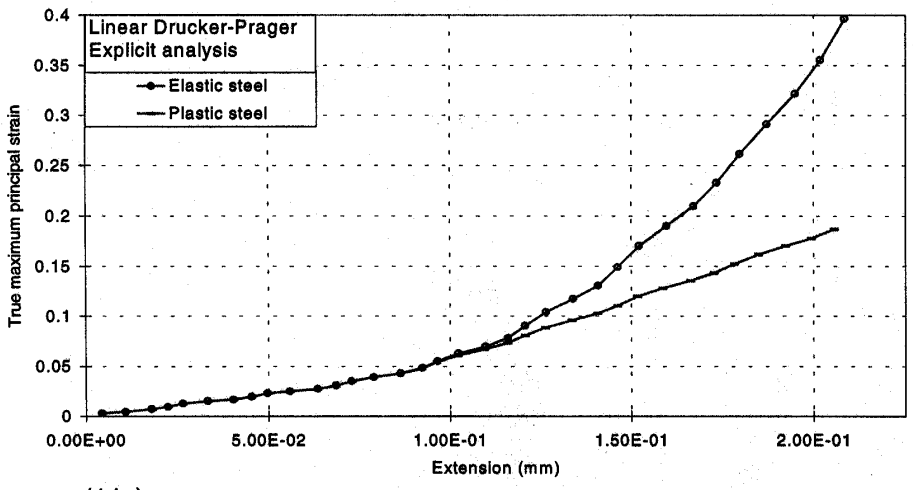

(14c)

Figure 14 Peak values of the maximum principal strain against extension using different analyses. (a) comparison of results obtained with the linear and exponent Drucker-Prager materials models. (b) comparison of results using quasi-static and dynamic analyses. (c) influence of steel plasticity.